J. Fluid Mech. (2001), *vol.* 438, *pp.* 363–377. Printed in the United Kingdom

Three-dimensional instability of axisymmetric flow in a rotating lid–cylinder enclosure

By A. Yu. GELFGAT, P. Z. BAR-YOSEPH AND A. SOLAN
Faculty of Mechanical Engineering, Technion, Israel Institute of Technology, Haifa 32000, Israel

(Received 16 May 2000 and in revised form 27 November 2000)

The axisymmetry-breaking three-dimensional instability of the axisymmetric flow between a rotating lid and a stationary cylinder is analysed. The flow is governed by two parameters – the Reynolds number Re and the aspect ratio γ (=height/radius). Published experimental results indicate that in different ranges of γ axisymmetric or non-axisymmetric instabilities can be observed. Previous analyses considered only axisymmetric instability. The present analysis is devoted to the linear stability of the basic axisymmetric flow with respect to the non-axisymmetric perturbations. After the linearization the stability problem separates into a family of quasi-axisymmetric subproblems for discrete values of the azimuthal wavenumber k. The computations are done using the global Galerkin method. The stability analysis is carried out at various densely distributed values of γ in the range $1 < \gamma < 3.5$. It is shown that the axisymmetric perturbations are dominant in the range $1.63 < \gamma < 2.76$. Outside this range, for $\gamma < 1.63$ and for $\gamma > 2.76$, the instability is three-dimensional and sets in with $k = 2$ and $k = 3$ or 4, respectively. The azimuthal periodicity, patterns, characteristic frequencies and phase velocities of the dominant perturbations are discussed.

1. Introduction

Many flows generated by rotation or natural convection in axisymmetric enclosures with axisymmetric boundary conditions break into non-axisymmetric patterns above a certain threshold of the governing parameters. Such axisymmetry-breaking instabilities are of interest in stability analysis and are of major importance in applications. Specifically, our attention is focused on cases when the non-axisymmetric patterns evolve from a non-trivial axisymmetric flow field, rather than from a state of rest. In such cases the basic flow is not known analytically *a priori* and must be computed for each value of the governing parameters. A time-dependent fully three-dimensional computation of the flow, searching for the appearance of an instability, involves a considerable computational effort and is not well-suited for a systematic parametric search for stability limits, in particular in the case of multiple solution branches.

In the present study we apply a global spectral method that consists of a Fourier expansion of the flow in the azimuthal direction and a Galerkin decomposition in the meridional plane. The three-dimensional linear stability problem then separates into a sequence of quasi-two-dimensional problems and allows the detailed evaluation of the stability thresholds and the multiplicity of the resulting flows. The present paper is a non-axisymmetric extension of our previous analysis of axisymmetric instabilities (Gelfgat, Bar-Yoseph & Solan 1996).

Rotating lid–cylinder systems have been studied extensively both numerically and experimentally, in particular in connection with vortex breakdown. In experiments,

the observed effects were axisymmetric and non-axisymmetric, steady and unsteady (Escudier 1984; Spohn, Mory & Hopfinger 1998; Roesner 1990; Stevens, Lopez & Cantwell 1999). This led to some controversy, but there are no reports of the detailed structure of the non-axisymmetric modes. Numerical analyses of the phenomenon were mainly axisymmetric, with studies of the transition from axisymmetric steady to axisymmetric unsteady oscillatory states, e.g. Daube & Sørensen (1989), Lopez (1990), Lopez & Perry (1992), Tsitverblit & Kit (1998), and Stevens *et al.* (1999). Most of these studies were by direct numerical simulation rather than by a stability analysis. In our previous paper (Gelfgat *et al.* 1996) we presented a comprehensive numerical stability analysis of the axisymmetric case by a spectral Galerkin method. In that paper the flow in a rotating lid–stationary cylinder enclosure was studied for a range of aspect ratios (height/radius) $1 \leqslant \gamma \leqslant 3.5$. The critical Reynolds number and the critical frequency of the perturbations were computed and several individual modes of axisymmetric instability were identified, in good agreement with the experimental results of Escudier (1984) in the range $1.86 < \gamma < 2.9$. Below $\gamma = 1.86$ no experimental results were available for comparison, while above $\gamma = 2.9$, for $2.9 < \gamma < 3.5$ our axisymmetric instability did not agree with Escudier's observation that 'for $\gamma > 3.1$ the first sign of non-steady motion is a precession of the lower breakdown structure'. Our conclusion there was that in that range of γ non-axisymmetric effects must be present. In a recent report on an experimental study of flow in a cylinder with rotating bottom and no-slip or stress-free upper boundary Spohn *et al.* (1998) observed non-axisymmetric results even in the range where previous analyses predicted an axisymmetric instability and they question the validity of such axisymmetric analyses. To our knowledge, no detailed analysis of non-axisymmetric instability for the swirling flows in a closed cylinder with rotating top/bottom has been published. It is the purpose of the present paper to present such a detailed analysis, allowing different azimuthal wavenumbers k and investigating which value of k is critical, i.e. has the lowest neutral Reynolds number corresponding to the growth of a particular mode with the azimuthal wavenumber k_{cr}. In particular, the analysis will show in what region of γ the axisymmetric instability ($k_{cr} = 0$) is, indeed, the most critical.

The outline of this paper is as follows: in § 2 the problem is formulated; in § 3 the spectral Galerkin method used is presented; in § 4 test calculations used for validation are reported; in § 5 we report the detailed results for axisymmetry-breaking instabilities in a cylinder with a rotating lid; § 6 summarizes the paper.

2. Formulation of the problem

We consider a vertical cylinder filled with an incompressible Newtonian fluid and covered by a lid, which rotates at a constant angular velocity Ω_0. Thus, the geometry and boundary conditions are steady and axisymmetric and can generate a steady and axisymmetric flow. The dimensionless momentum and continuity equations are

$$\frac{\partial \boldsymbol{v}}{\partial t} + (\boldsymbol{v} \cdot \nabla)\boldsymbol{v} = -\nabla p + \frac{1}{Re}\Delta \boldsymbol{v}, \tag{1}$$

$$\nabla \cdot \boldsymbol{v} = 0, \tag{2}$$

where $\boldsymbol{v}$ is the velocity, p the pressure, $Re = \Omega_0 R^2/\nu$ the Reynolds number, R the radius of the cylinder, and ν is the kinematic viscosity. An additional governing parameter is the aspect ratio $\gamma = H/R$, where H is the height of the cylinder. The velocity, pressure, time and length are scaled by $\Omega_0 R$, $\rho(\Omega_0 R)^2$, R^2/ν and R, respectively (ρ is the density).

The boundary conditions are

$$u = v = w = 0 \quad \text{at} \quad z = 0 \quad \text{and at} \quad r = 1 \quad \text{(stationary cylinder)}, \tag{3a}$$

$$u = w = 0, \quad v = r \quad \text{at} \quad z = \gamma \quad \text{(rotating lid)}. \tag{3b}$$

We denote by $\boldsymbol{V}(r,z) = \{U(r,z), V(r,z), W(r,z)\}$, and $P(r,z)$ the basic axisymmetric steady flow which corresponds to the solution of the axisymmetric part of the system (1)–(3). Consider infinitely small perturbations $\tilde{\boldsymbol{v}} = \{\tilde{u}, \tilde{v}, \tilde{w}\}$ and $\tilde{p}$ of the velocity and the pressure, respectively, which depend on the three coordinates (r, ϕ, z) and time t. The linearized problem for the perturbations is

$$\frac{\partial \tilde{\boldsymbol{v}}}{\partial t} + (\boldsymbol{V} \cdot \nabla)\tilde{\boldsymbol{v}} + (\tilde{\boldsymbol{v}} \cdot \nabla)\boldsymbol{V} = -\nabla \tilde{p} + \frac{1}{Re}\Delta \tilde{\boldsymbol{v}}, \tag{4}$$

$$\nabla \cdot \tilde{\boldsymbol{v}} = 0, \tag{5}$$

with the homogeneous no-slip boundary conditions

$$\tilde{\boldsymbol{v}} = \boldsymbol{0} \quad \text{on all boundaries.} \tag{6}$$

To complete the formation we add conditions of 2π-periodicity of all the functions

$$f(\phi + 2\pi) = f(\phi), \tag{7}$$

where f represents one of the functions $\tilde{u}$, $\tilde{v}$, $\tilde{w}$ or $\tilde{p}$.

According to linear stability theory, we assume the time dependence of the perturbation functions $\{\tilde{u}, \tilde{v}, \tilde{w}, \tilde{p}\}$ as $\sim \exp(\lambda t)$, where λ is an eigenvalue of the linear homogeneous problem (4)–(7). The periodicity conditions (7) allow us to represent the solution of (4)–(7) as Fourier series in the azimuthal direction. Thus, the perturbation functions can be represented as

$$\{\tilde{u}, \tilde{v}, \tilde{w}, \tilde{p}\} = \exp(\lambda t) \sum_{k=-\infty}^{k=\infty} \{u_k(r,z), v_k(r,z), w_k(r,z), p_k(r,z)\} \exp(\mathrm{i}k\phi). \tag{8}$$

The integer number k in (8) is an azimuthal wavenumber. The value $k = 0$ corresponds to an axisymmetric perturbation. The equations for the Fourier coefficients $\{u_k, v_k, w_k, p_k\}$ are obtained after substitution of (8) into (4)–(7). The axisymmetric functions $\{u_k, v_k, w_k, p_k\}$ define the eigenvector of (4)–(7) for each eigenvalue $\lambda(k)$.

The equations resulting from the last substitution contain terms proportional to $1/r^2$, which represent a non-integrable singularity at $r = 0$. This singularity is an artifact introduced by the use of polar coordinates in the (r, ϕ)-plane. To see how this singularity can be eliminated, we bring the equations into the following form, using the continuity equation to substitute for $(2\mathrm{i}ku_k/r^2)$ and $(2\mathrm{i}kv_k/r^2)$:

$$\lambda u_k + U\frac{\partial u_k}{\partial r} + W\frac{\partial u_k}{\partial z} + u_k\frac{\partial U}{\partial r} + w_k\frac{\partial U}{\partial z} + \frac{\mathrm{i}k}{r}Vu_k - \frac{2Vv_k}{r}$$
$$= -\frac{\partial p_k}{\partial r} + \frac{1}{Re}\left(\frac{\partial^2 u_k}{\partial r^2} + \frac{3}{r}\frac{\partial u_k}{\partial r} - \frac{k^2-1}{r^2}u_k + \frac{\partial^2 u_k}{\partial z^2} + \frac{2}{r}\frac{\partial w_k}{\partial z}\right), \tag{9}$$

$$\lambda v_k + U\frac{\partial v_k}{\partial r} + W\frac{\partial v_k}{\partial z} + u_k\frac{\partial V}{\partial r} + w_k\frac{\partial W}{\partial z} + \frac{\mathrm{i}k}{r}Vv_k - \frac{Uv_k}{r} - \frac{Vu_k}{r}$$
$$= -\frac{\mathrm{i}k}{r}p_k + \frac{1}{Re}\left(\frac{\partial^2 v_k}{\partial r^2} + \frac{1}{r}\frac{\partial v_k}{\partial r} + \frac{k^2-1}{r^2}v_k + \frac{\partial^2 v_k}{\partial z^2} - \frac{2\mathrm{i}k}{r}\frac{\partial u_k}{\partial r} - \frac{2\mathrm{i}k}{r}\frac{\partial w_k}{\partial z}\right), \tag{10}$$

$$\lambda w_k + U\frac{\partial w_k}{\partial r} + W\frac{\partial w_k}{\partial z} + u_k\frac{\partial W}{\partial r} + w_k\frac{\partial W}{\partial z} + \frac{\mathrm{i}k}{r}Vw_k$$
$$= -\frac{\partial p_k}{\partial z} + \frac{1}{Re}\left(\frac{\partial^2 w_k}{\partial r^2} + \frac{1}{r}\frac{\partial w_k}{\partial r} - \frac{k^2}{r^2}w_k + \frac{\partial^2 w_k}{\partial z^2}\right). \tag{11}$$

It is easy to see now that terms proportional to $1/r^2$ vanish if (Gelfgat *et al.* 1999)

$$u_0 = 0, \quad v_0 = 0, \quad w_0 \neq 0, \qquad u_{\pm1} \neq 0, \quad v_{\pm1} \neq 0, \quad w_{\pm1} = 0, \tag{12a}$$
$$u_k = v_k = w_k = 0 \quad \text{for} \quad |k| > 1. \tag{12b}$$

3. Numerical method

The axisymmetric basic-flow problem together with the three-dimensional linear stability problem (9)–(11) are solved using the spectral Galerkin method. The axisymmetric part of the numerical method and its application to a numerical study of the swirling flow in a cylinder with rotating lid is described in Gelfgat *et al.* (1996). Here we focus only on the three-dimensional part of the numerical method. The formulation of the method consists of three parts: (*a*) definitions of the basis functions, (*b*) formulae for the calculations of the Galerkin projections of the linear and nonlinear (bilinear in our case) terms, and (*c*) the final dynamical system and computational procedure. Parts (*a*) and (*c*) are described below. Part (*b*), which is technical and lengthy, is omitted.†

3.1. *Basis functions*

The system of basis functions of the Galerkin method is split into an axisymmetric and a non-axisymmetric subsystem. This allows us to extract the axisymmetric problem for the basic flow as a separate part and then consider the three-dimensional stability problem. To do this we consider an arbitrary three-dimensional velocity field $\boldsymbol{v} = (u, v, w)$ and notice that due to continuity (equation (2)) among the three components u, v and w only two are independent:

$$\begin{Bmatrix} u(r,\phi,z) \\ v(r,\phi,z) \\ w(r,\phi,z) \end{Bmatrix} = \begin{Bmatrix} u \\ -r\int\left[\dfrac{\partial u}{\partial r} + \dfrac{u}{r}\right]\mathrm{d}\phi \\ 0 \end{Bmatrix} + \begin{Bmatrix} 0 \\ -r\int\dfrac{\partial w}{\partial z}\mathrm{d}\phi \\ w \end{Bmatrix}. \tag{13}$$

Obviously, the velocity components u and w consist of the axisymmetric and non-axisymmetric parts. The axisymmetric part of v can be associated with the ϕ-independent 'constant' of integration in (13). Let us introduce an additional axisymmetric vector $\boldsymbol{A}(r,z,t)$ containing the axisymmetric parts of u, v and w. The remaining non-axisymmetric parts of the right-hand side of (13) will be denoted as vectors $\boldsymbol{B}(r,\phi,z,t)$ and $\boldsymbol{C}(r,\phi,z,t)$. Then (13) can be represented as

$$\boldsymbol{v}(r,\phi,z,t) = \boldsymbol{A}(r,z,t) + \boldsymbol{B}(r,\phi,z,t) + \boldsymbol{C}(r,\phi,z,t)$$
$$= \begin{Bmatrix} A^r(r,z,t) \\ A^\phi(r,z,t) \\ A^z(r,z,t) \end{Bmatrix} + \begin{Bmatrix} B^r(r,\phi,z,t) \\ B^\phi(r,\phi,z,t) \\ 0 \end{Bmatrix} + \begin{Bmatrix} 0 \\ C^\phi(r,\phi,z,t) \\ C^z(r,\phi,z,t) \end{Bmatrix}. \tag{14}$$

† Details can be obtained from the authors or the *JFM* Editorial Office, or found at http://tx.technion.ac.il/~cml/cml/staff/publicat.htm

Thus, $\boldsymbol{A}(r,z,t)$ represents the axisymmetric part of the flow, which is a projection of the three-dimensional flow on the (r,z)-plane. The second and the third terms. $\boldsymbol{B}(r,\phi,z,t)$ and $\boldsymbol{C}(r,\phi,z,t)$ can be interpreted as projections of the flow on the (r,ϕ)- and (z,ϕ)-coordinate surfaces respectively. Note that the component A^{ϕ} represents the axisymmetric swirl and, within the axisymmetric model, should be defined as a separate scalar function. The components A^{r} and A^{z} must satisfy the continuity equation (2) and therefore should form an axisymmetric vector which we denote as $\boldsymbol{A}^{(r,z)}$. Finally, the Galerkin–Fourier expansions for the functions $\boldsymbol{A}, \boldsymbol{B}$ and $\boldsymbol{C}$ can be defined as

$$\boldsymbol{A}(r,z,t) = A^{\phi}(r,z,t)\boldsymbol{e}_{\phi} + \boldsymbol{A}^{(r,z)}(r,z,t), \tag{15}$$

$$A^{\phi}(r,z,t) = \Omega(r,z) + r\sum_{i=0}^{N_r}\sum_{j=0}^{N_z} D_{ij}(t)\Phi_{ij}(r,z), \tag{16}$$

$$\boldsymbol{A}^{(r,z)}(r,z,t) = \sum_{i=1}^{M_r}\sum_{j=1}^{M_z} A_{ij}(t)\boldsymbol{U}_{ij}(r,z), \tag{17}$$

$$\boldsymbol{B}(r,\phi,z,t) = \sum_{\substack{k=-\infty \\ k\neq 0}}^{k=+\infty}\sum_{i=1}^{N_r}\sum_{j=1}^{N_z} B_{ijk}(t)\boldsymbol{V}_{ijk}(r,z)\exp(\mathrm{i}k\phi), \tag{18}$$

$$\boldsymbol{C}(r,\phi,z,t) = \sum_{\substack{k=-\infty \\ k\neq 0}}^{k=+\infty}\sum_{i=1}^{N_r}\sum_{j=1}^{N_z} C_{ijk}(t)\boldsymbol{W}_{ijk}(r,z)\exp(\mathrm{i}k\phi). \tag{19}$$

Here $A_{ij}(t), B_{ijk}(t), C_{ijk}(t)$, and $D_{ij}(t)$ are unknown time-dependent coefficients, A^{ϕ} is the axisymmetric part of the azimuthal velocity and $\boldsymbol{A}^{(r,z)}$ is the axisymmetric meridional part of the flow. The scalar components of the vector basis functions $\boldsymbol{U}_{ij}, \boldsymbol{V}_{ijk}, \boldsymbol{W}_{ijk}$, and Φ_{ij} are defined as linear superpositions of Chebyshev polynomials (for details see Gelfgat *et al.* 1999). The function $\Omega(r,z)$ is used to exactly satisfy the non-homogeneous boundary conditions for the azimuthal velocity. Details can be found in Gelfgat *et al.* (1996).

The three-dimensional Galerkin–Fourier series defined by (14)–(19) are used here for the calculation of the three-dimensional linear perturbation equations only. However, they can be used for the solution of the full nonlinear three-dimensional problems as well.

3.2. *Nonlinear dynamical system and computational procedure*

The nonlinear dynamical system for the time-dependent coefficients of the Galerkin series (15)–(19) has the following form (the summation convention over repeating indices is assumed):

$$\frac{\partial Z_i(t)}{\partial t} = L_{ij}Z_j(t) + N_{ijk}Z_j(t)Z_k(t) + F_i, \tag{20}$$

where the vector $\boldsymbol{Z}(t)$ contains the components of all the coefficients $A_{nm}(t)$, $B_{nmk}(t)$, $C_{nmk}(t)$ and $D_{nm}(t)$, and the matrices $\boldsymbol{L}$, $\boldsymbol{N}$ and $\boldsymbol{F}$ contain Galerkin projections of linear, bilinear and source terms respectively (e.g. the term Ω^2/r following from decomposition (16)). The matrices $\boldsymbol{L}$, $\boldsymbol{N}$ and $\boldsymbol{F}$ depend on the governing parameters and the azimuthal wavenumber.

Suppose that the vector $\boldsymbol{X}$ contains all the coefficients A_{nm}, corresponding to the steady axisymmetric solution of a problem, i.e. the steady solution of (20) for $k = 0$, ($B_{ij0} = C_{ij0} = 0$ for an axisymmetric solution). Assume also, that the vector $\boldsymbol{z}$ contains all the coefficients A_{nm}, B_{ijk} and C_{ijk} of a three-dimensional perturbation. Then the linearized stability problem (4) for the steady solution $\boldsymbol{X}$ becomes

$$\lambda z_i = L_{ij} z_j + (N_{ijk} + N_{ikj}) X_j z_k, \tag{21}$$

where it is already assumed that for an infinitely small perturbation $z_i(t) = z_i \exp(\lambda t)$. According to the linear stability theory, the steady solution $\boldsymbol{X}$ is unstable if there exists at least one eigenvalue of (21) λ, whose real part is positive: $\mathrm{Re}(\lambda) > 0$.

Investigation of stability requires determining the values of the governing parameters such that the real part of the dominant eigenvalue (eigenvalue with the largest real part) $\Lambda = \Lambda^r + \mathrm{i}\Lambda^i$ is zero: $\Lambda^r = 0$. If for some values of the governing parameters the dominant eigenvalue has zero real part $\Lambda^r = 0$ and $\partial\Lambda^r/\partial Re \neq 0$, then $\Lambda^i \neq 0$ means a bifurcation to a periodic solutions, i.e. a Hopf bifurcation, and $\Lambda^i = 0$ indicates a bifurcation from one steady solution to another. In the case $\Lambda^i \neq 0$ the imaginary part Λ^i of the dominant eigenvalue gives the circular frequency of the oscillatory solution that branches from the steady state after the onset of the oscillatory instability. The eigenvector $\boldsymbol{z}$ that corresponds to the dominant eigenvalue Λ with $\Lambda^r = 0$ defines the most unstable perturbation of system (21). The most unstable perturbation of the flow can be calculated using the series (14)–(18) with coefficients A_{nm}, B_{nmk}, C_{nmk} and D_{nm} defined as components of the eigenvector $\boldsymbol{z}$. In the same way the limit cycle of the dynamical system (20), which develops as a result of Hopf bifurcation, defines an approximation of the periodic solution of problem (1)–(3).

The whole computational procedure, similar to that in our previous paper (Gelfgat *et al.* 1996), is as follows. A steady axisymmetric solution of (20) is calculated using the Newton method. Then the eigenvalue problem (21) is solved for a certain value of Reynolds number Re^0. The eigenvalues and eigenvectors of (21) are calculated by the QR algorithm. These two steps are repeated for the next value of the Reynolds number, usually $1.01Re^0$. Then the real part of the dominant eigenvalue $\Lambda^r(k, Re)$ is considered as a function of the Reynolds number, and the value of the neutral Reynolds number $Re_n(k)$ corresponding to $\Lambda^r(k, Re_n) = 0$ is calculated by the secant method for each azimuthal wavenumber k. The critical Reynolds number of the flow is defined as $Re_{cr} = \min_k Re_n(k)$. The value of k corresponding to the minimum of $Re_n(k)$ is then the critical (the most dangerous) azimuthal wavenumber k_{cr}. Thus, the calculation of a critical parameter requires a series of calculations for different values of k. As a rule, the calculations are continued until a minimum on the curve $Re_{cr}(k)$ and the behaviour of $Re_n(k)$ for large k are found.

4. Code validation

The validation of the computational procedure was performed in several steps. First, the Galerkin projections of the linear terms were validated by the solution of the classical Rayleigh–Bénard problem for convective stability of quiescent fluid in a vertical cylinder heated from below. The results of Hardin *et al.* (1990) for a stationary cylinder, and Jones & Moore (1979) and Goldstein *et al.* (1993) for a rotating cylinder were used for the comparison. It was found that the dominant mode converges already for 10×10 functions. The details can be found in Gelfgat & Tanasawa (1993).

	$k=1$		$k=2$		$k=3$		$k=4$		$k=5$	
	Re_n	ω_n	Re_n	ω_n	Re_n	ω_n	Re_n	ω_n	Re_n	ω_n
10×10	3554	−0.2878	3948	−0.03369	3187	−0.2967	3021	−0.4188	3185	−0.5487
20×20	3969	0.07396	4033	−0.03286	2758	−0.2954	2927	−0.4116	3174	−0.5769
30×30	3973	0.07361	4030	−0.03289	2777	−0.2953	2940	−0.4123	3204	−0.5782
40×40	3973	0.07349	4030	−0.03289	2765	−0.2953	2934	−0.4123	3203	−0.5781
	$k=6$		$k=7$		$k=8$		$k=9$		$k=10$	
	Re_n	ω_n	Re_n	ω_n	Re_n	ω_n	Re_n	ω_n	Re_n	ω_n
10×10	3477	−0.6842	3684	−0.8218	4362	−0.9594	4968	−1.0955	5569	−1.230
20×20	3306	−0.7009	3531	−0.8283	3819	−0.9579	4161	−1.089	4576	−1.222
30×30	3347	−0.7020	3553	−0.8284	3802	−0.9573	4107	−1.089	4497	−1.223
40×40	3346	−0.7018	3548	−0.8285	3795	−0.9571	4099	−1.089	4505	−1.223

TABLE 1. Convergence of the neutral Reynolds number and the neutral frequency of oscillations for different numbers of basis functions and $\gamma = 3.25$. Axisymmetric base flow is calculated with 30×30 basis functions.

Second, the Galerkin projections of bilinear terms were validated by a check of the energy conservation of the convective momentum transport

$$\langle(\boldsymbol{v}\cdot\nabla)\boldsymbol{v},\boldsymbol{v}\rangle = \int_V [(\boldsymbol{v}\cdot\nabla)\boldsymbol{v}]\cdot\boldsymbol{v}\,\mathrm{d}V = 0, \tag{22}$$

which holds for any divergence-free velocity field satisfying no-penetration boundary conditions. To validate the bilinear terms in (20) the vector $\boldsymbol{V}+\tilde{\boldsymbol{v}}$ was substituted in (22) instead of $\boldsymbol{v}$. Obviously, the relation (22) must hold for each basis function satisfying the continuity equation and the boundary conditions, as well as for any linear superposition of these functions. The latter was checked by the evaluation of the corresponding integrals during the computational process.†

Third, we used as a test problem the axisymmetry-breaking bifurcation of steady non-rotating convective flow in a vertical cylinder heated from below. This was compared with the numerical results of Neumann (1990) and Wanschura, Kuhlmann & Rath (1996). The results of the comparison were favourable (the deviation for the critical Rayleigh number was about 1%), and have already been reported in Gelfgat *et al.* (1999). In that paper we also reported a comparison with the experiment which showed a high-wavenumber axisymmetry splitting in free convection. The computation and the experiment showed similar results, with difference in detail due to the fact that the supercriticality of the experiment was relatively high.

Finally, convergence tests with respect to the number of basis functions were performed for the problem considered here. The convergence of the axisymmetric steady states has already been studied in Gelfgat *et al.* (1996) and the results were compared with solutions obtained by the finite volume method. It was found that truncation up to 30×30 basis functions in the r- and z-directions, respectively, provides considerably good accuracy (e.g. 3 correct decimal digits for maximal value of the stream function and coordinates of the maximum). In the present study we focused on the convergence of critical parameters corresponding to the three-dimensional perturbations. Table 1 shows Re_{cr} and the neutral frequency of oscillations ω_{cr}

† Technical details can be obtained from the authors or the *JFM* Editorial Office, or found at http://tx.technion.ac.il/~cml/cml/staff/publicat.htm

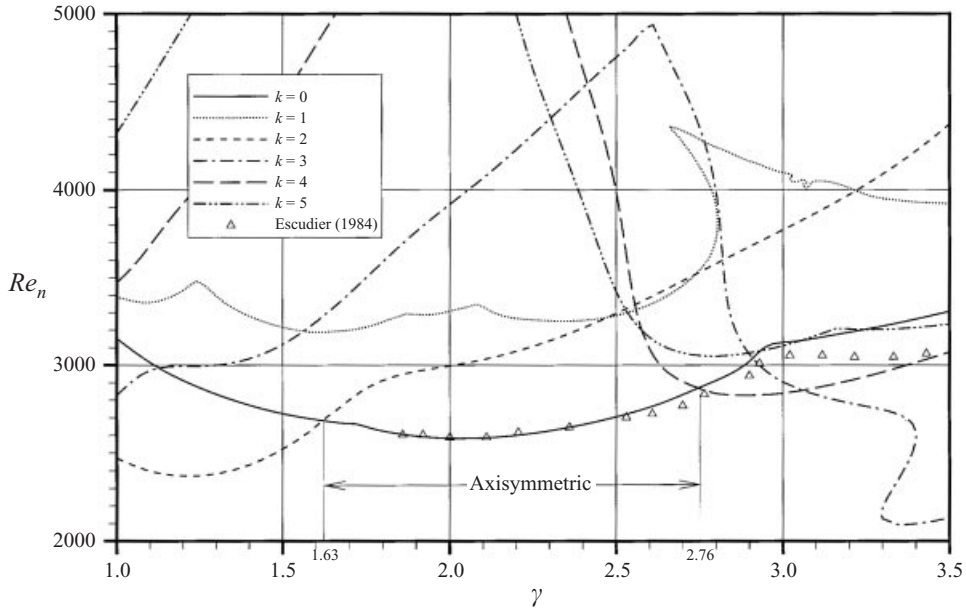

FIGURE 1. Neutral and critical Reynolds numbers $Re_n(\gamma,k)$ and $Re_{cr}(\gamma,k)$.

computed for $\gamma = 3.25$ and $k = 1$–10 using 10×10, 20×20, 30×30, and 40×40 basis functions. The basic flow was computed using 30×30 functions. It is seen that convergence is satisfactory.

5. Axisymmetry breaking in a cylinder with rotating lid: results

To study the stability of the flow in a cylinder with rotating lid the aspect ratio γ was fixed at various (densely distributed) values in the range $1 \leqslant \gamma \leqslant 3.5$. In this range experimental results are available in the literature (Escudier 1984; Spohn *et al.* 1998). At each γ various integer values of the azimuthal wavenumber k were chosen in the range $0 \leqslant k \leqslant 5$† and the neutral values $Re_n(\gamma,k)$ and $\omega_n(\gamma,k)$ were computed (figures 1 and 2). Thus, at each γ, the most unstable mode can be recognized as that corresponding to the lowest Re_n, i.e. $Re_{cr}(\gamma) = \min_k Re_n(\gamma,k)$.

The curves $Re_n(\gamma,k)$ consist of several continuous branches. Each continuous branch corresponds to a certain pattern of the three-dimensional perturbation (figures 3–5). Different perturbation patterns (eigenvectors of the linearized problem) correspond to different eigenvalues of (21). Therefore, the breaks of the neutral curves $Re_n(\gamma,k)$ are accompanied by abrupt changes in $\omega_n(\gamma,k)$. A similar result with several separate branches (for different regions of γ) was obtained for the axisymmetric case by Gelfgat *et al.* (1996).

The perturbation $f(r,z,\phi;k)$ of each axisymmetric scalar function $F(r,z)$ can be represented as

$$f(r,z,\phi,t;k) = a\{f_k(r,z)\exp[\mathrm{i}(k_{cr}\phi + \omega_{cr}t)] + f_{-k}(r,z)\exp[\mathrm{i}(-k_{cr}\phi - \omega_{cr}t)]\}. \quad (23)$$

Here a is an undetermined perturbation amplitude and the imaginary pairs $\pm(\mathrm{i}k_{cr}, \mathrm{i}\omega_{cr})$ correspond to the complex eigenpair of (4). Considering the complex conjugate of

† Our test calculations showed that Re_n increases with k for $5 \leqslant k \leqslant 10$. Therefore we carried out a detailed parametric study only for $0 \leqslant k \leqslant 5$.

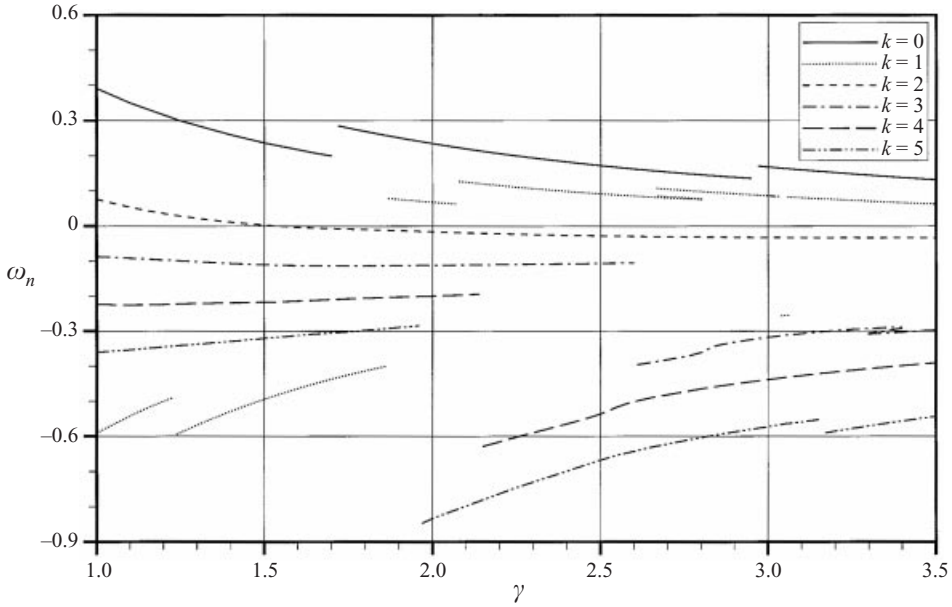

FIGURE 2. Frequency $\omega_n(\gamma, k)$.

the perturbation equations (9)–(11) it can be shown that $f_k = -\bar{f}_{-k}$ (overbar denotes the complex conjugate), which makes the expression (23) real. Therefore, it suffices to calculate the critical values for positive k only.

For $\omega_{cr} \neq 0$, the instability sets in as an azimuthal travelling wave. The sign of ω_{cr} shows the azimuthal direction of wave propagation with respect to the direction of the lid rotation. We always assume that $\Omega_0 > 0$, which corresponds to the counter-clockwise rotation of the lid. Therefore, the azimuthal wave propagates in the direction of the lid rotation when $\omega_{cr} > 0$, and in the opposite direction when $\omega_{cr} < 0$. Thus, in the case of three-dimensional axisymmetry-breaking instability the critical frequency represents not only the time-dependence, but also the direction and the angular phase velocity of the azimuthal travelling wave defined as $c = \omega_{cr}/k$ ($k \neq 0$).

Consider figure 1, which shows $Re_n(\gamma, k)$ for $1 \leqslant \gamma \leqslant 3.5$ and $0 \leqslant k \leqslant 5$ together with the experimental results of Escudier (1984). Note the crossovers of the stability curves for different k, which indicate that in different ranges of the aspect ratio γ different values of the wavenumber k are the most dangerous (lowest Re_n). Consider also figure 2, where for almost all parameter values $\omega_n \neq 0$, which for all $k \neq 0$ indicates an azimuthally travelling wave. Finally, note that the experimental results are available only in the range $1.86 \leqslant \gamma \leqslant 3.5$.

In the range $1.63 \leqslant \gamma \leqslant 2.76$ our calculations predict that the dominant perturbation mode is axisymmetric ($k = 0$), in agreement with the experimental observations of Escudier (1984) and with our previous analysis (Gelfgat *et al.* 1996) in which only axisymmetric perturbations were allowed. This result also answers the question raised by Spohn *et al.* (1998) regarding the symmetry properties of the instability that they observed near $\gamma = 1.75$ and $Re = 1850$ – our present results re-validate the existence of an axisymmetric instability near that point (see further discussion below).

Outside the range $1.63 \leqslant \gamma \leqslant 2.76$ the instability is non-axisymmetric. This conclusion is supported by recent three-dimensional calculations of Blackburn & Lopez (2000) who found that at $\gamma = 2.5$ the primary oscillatory instability sets in at $Re \approx 2700$

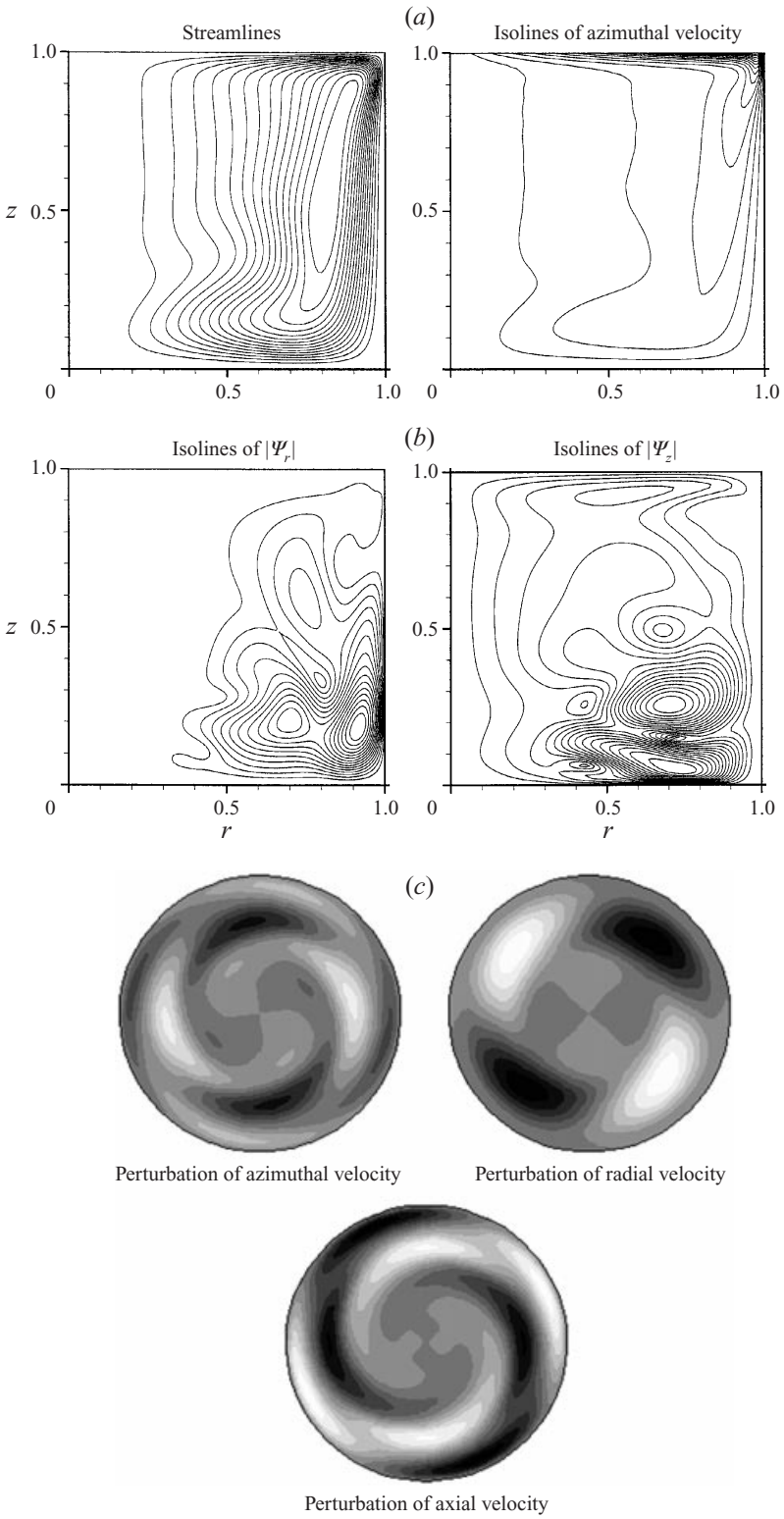

FIGURE 3. For caption see facing page.

and leads to the development of oscillatory axisymmetric flow. Our result for this case (Gelfgat *et al.* 1996) is $Re_{cr} = 2706$.

Unfortunately, there are no independent experimental or three-dimensional numerical data regarding the onset of instability at $\gamma \leqslant 1.63$. Above $\gamma = 2.76$ our results disagree with the experimental data of Escudier (1984). Escudier observed transition from steady axisymmetric to non-axisymmetric oscillatory states for $\gamma \geqslant 3.0$, while the present results give the slightly lower value $\gamma \approx 2.76$. Another difference is the value of the critical Reynolds numbers for $\gamma > 3$ (see figure 1). Furthermore, there is no agreement in the pattern of the supercritical axisymmetric oscillatory state: Escudier observed the lower flow structure precessing around the axis, which could correspond to a perturbation with $k = 1$. Our results predict $k = 3$ or 4. However, at $\gamma = 3.1$ and $Re > 3000$, where Escudier observed the rotating structure, the parameters are above the stability limits for $k = 3$ and 4. Possibly, the experimental observation corresponds to a nonlinear interaction of these modes which includes, among other combinations, the mode $k = 1(4 - 3 = 1)$ through nonlinear interaction.

Below $\gamma \sim 1.63$ our calculations predict that the $k = 2$ mode is the most critical. Escudier's results do not refer to this range of γ. The time-integration of the full three-dimensional problem, performed by J. M. Lopez (2000, personal communication), shows that at $\gamma = 1.4$ and 1.65 the critical non-axisymmetric mode is $k = 2$, while at $\gamma > 2.9$ the critical modes are $k = 3$ or 4. The time-integration of the linearized and full three-dimensional problems, performed recently by O. Daube (2000, personal communication) for $\gamma = 1$ also showed that the critical mode is $k = 2$. The critical Reynolds numbers, obtained in the above studies, also agree with the present results. This adds more confidence in the results described.

To illustrate the details of the flow at the critical points, three representative cases, which lead to different wavenumbers, namely $k = 2$, 3, and 4, were chosen (figures 3–5). For each case we show the streamlines and isolines of the azimuthal velocity of the unperturbed axisymmetric basic flow and patterns of the non-axisymmetric perturbation velocity. The perturbation is represented in terms of the vector potential $\boldsymbol{\Psi}$ which is defined as

$$\boldsymbol{v} = \mathrm{rot}\,\boldsymbol{\Psi}, \quad u = \frac{1}{r}\frac{\partial \Psi_z}{\partial \phi} - \frac{\partial \Psi_\phi}{\partial z}, \quad v = \frac{\partial \Psi_r}{\partial z} - \frac{\partial \Psi_z}{\partial r}, \quad w = \frac{1}{r}\left(\frac{\partial r\Psi_\phi}{\partial r} - \frac{\partial \Psi_r}{\partial \phi}\right). \quad (24)$$

The component Ψ_ϕ represents the axisymmetric part of the flow. In purely axisymmetric flow Ψ_ϕ is the streamfunction. The components Ψ_r and Ψ_z represent the non-axisymmetric part of the flow and are defined by the basis function $\boldsymbol{V}_{ijk}$ and $\boldsymbol{W}_{ijk}$ respectively. Thus, the non-axisymmetric perturbation of the velocity can be described by the two components of the vector potential, instead of three components of the velocity. To illustrate the region of high fluctuation, we plot the moduli of the functions $|\Psi_r|$ and $|\Psi_z|$, which are independent of ϕ (figures 3*b*–5*b*). By comparison with the streamlines and isolines of the azimuthal velocity of the basic flow (figures 3*a*–5*a*) one can see that the instability always appears in the lower part of the cylinder where the rotation is weak and the meridional flow is directed from the sidewall towards the axis. The amplitudes of the perturbation of Ψ_r are strongest near the lower part of the sidewall. It is interesting that the axisymmetric perturbations reported

FIGURE 3. Flow patterns at the critical point. $\gamma = 1$, $k_{cr} = 2$ ($Re_{cr} = 2471$, $\omega_{cr} = 0.0766$): (*a*) streamlines and isolines of azimuthal velocity of basic flow, (*b*) isolines of $|\Psi_r|$ and $|\Psi_z|$ (amplitudes of perturbation vector potential), (*c*) perturbation velocity components at $z = \gamma/4$.

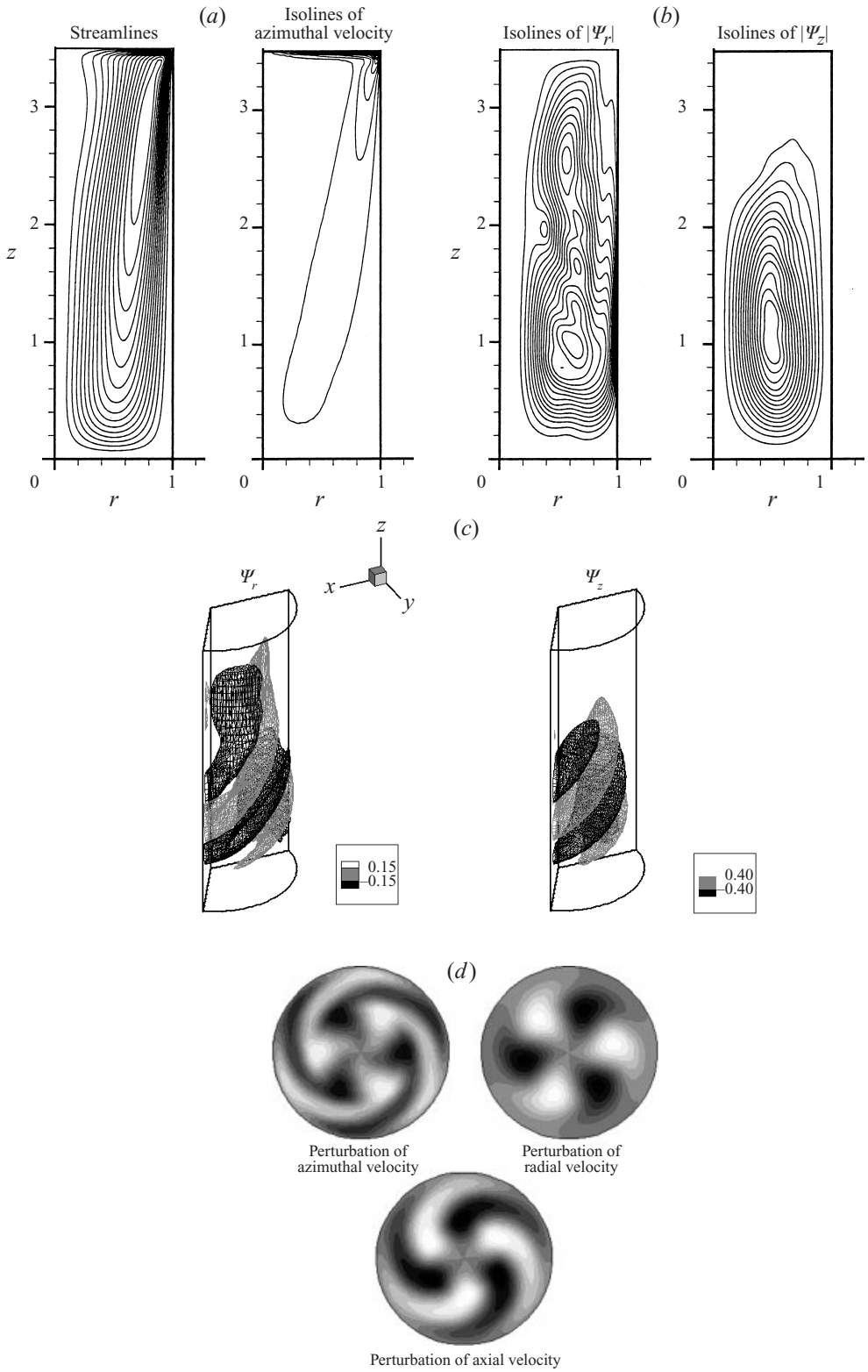

FIGURE 4. For caption see facing page.

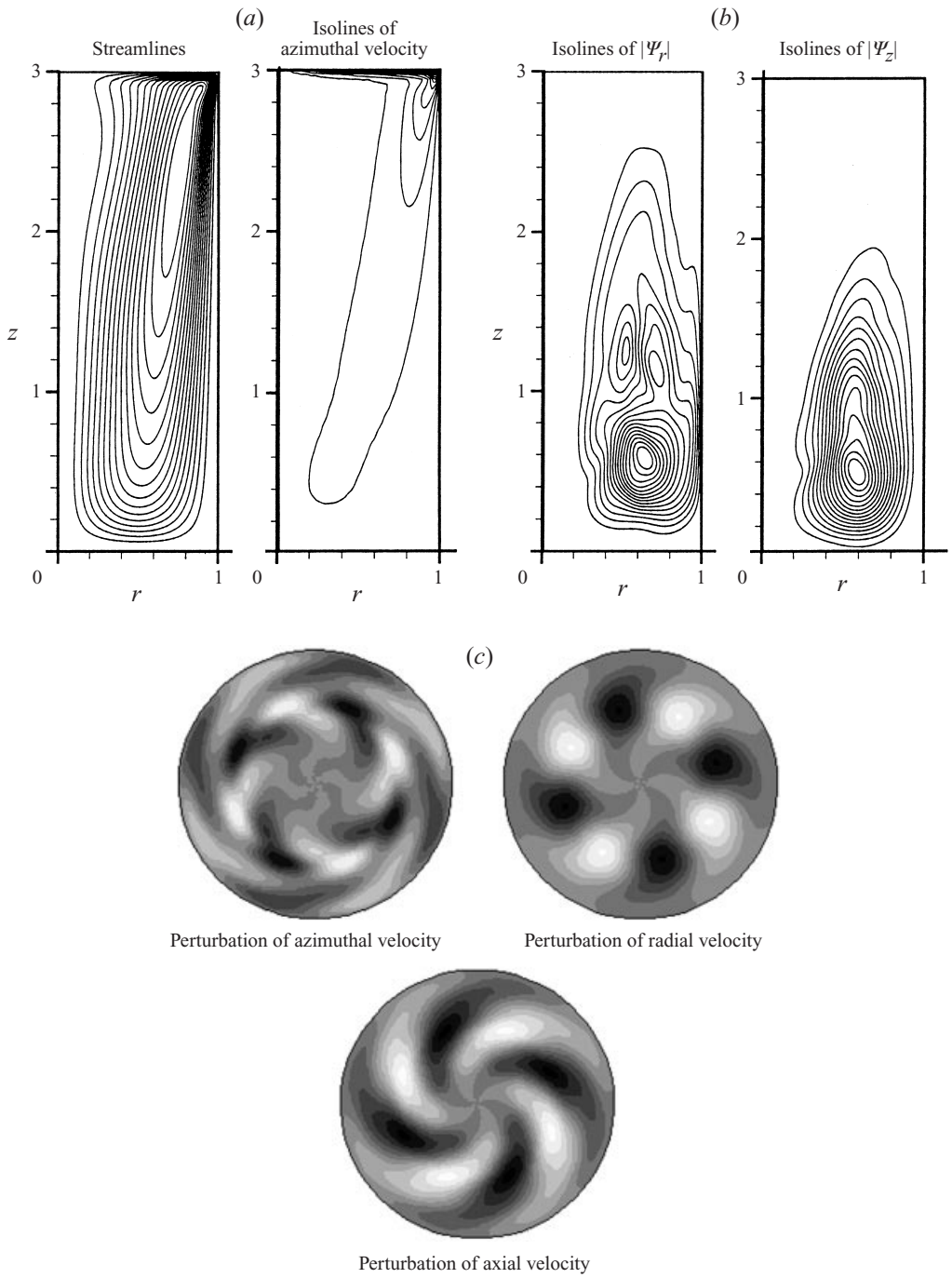

FIGURE 5. As figure 3, $\gamma = 3$, $k_{cr} = 4$ ($Re_{cr} = 2839$, $\omega_{cr} = -0.4386$).

FIGURE 4. Flow patterns at the critical point. $\gamma = 3.5$, $k_{cr} = 3$ ($Re_{cr} = 2132$, $\omega_{cr} = -0.2970$): (*a*) streamlines and isolines of azimuthal velocity of basic flow, (*b*) isolines of $|\Psi_r|$ and $|\Psi_z|$ (amplitudes of perturbation vector potential), (*c*) isosurfaces of Ψ_r and Ψ_z in sector of angle $2\pi/k$, (*d*) perturbation velocity components at $z = \gamma/4$.

by Gelfgat *et al.* (1996) had similar features. To illustrate the travelling waves we show perturbations of the velocity components plotted at the cross-sections $z = \gamma/4$ (figures 3*c*, 4*d*, 5*c*). The direction of the azimuthal travelling wave is counter-clockwise in figure 3 ($\omega_{cr} > 0$) and clockwise in figures 3, 4 and 5 ($\omega_{cr} < 0$).

The present three-dimensional analysis confirms, as did our previous result (Gelfgat *et al.* 1996), that the onset of the instability is not connected with the vortex breakdown that can occur in this system. Furthermore, for $\gamma > 3$ the observed three-dimensional instability sets in before the vortex breakdown occurs.

6. Conclusions

The method and results presented here show that the problem of axisymmetry breaking of a numerically calculated axisymmetric confined flow admits a complete and exact analysis by a combination of Fourier decomposition in the azimuthal direction and Galerkin decomposition in the azimuthal plane. The total analytical and numerical effort allows a systematic study of the neutral curves. The application of the method to the flow in a rotating lid–cylinder enclosure yields the critical Reynolds number as a function of the aspect ratio, as well as the critical modes. These results show that there exists a rather large variety of possible modes, with intricate crossovers and possible nonlinear interactions. These results may be of practical importance in the design of apparatus when such instabilities are to be avoided. The method may be further extended to other problem with similar symmetries, including heat/mass transfer, the MHD effect, more complicated rotation, etc. Comparison with the limited experimental data available shows agreement in certain cases and some disagreement in others, which may call for further experiments.

This research was supported by the Israel Science Foundation under Grant 110/96, by the Israel Ministry of Immigrant Absorption (to A. Gelfgat), and by the Winograd Chair of Fluid Mechanics and Heat Transfer at Technion.

REFERENCES

Blackburn, H. M. & Lopez, J. M. 2000 Symmetry breaking of the flow in a cylinder driven by a rotating endwall. *Phys. Fluids* **11**, 2698–2701.

Daube, O. & Sørensen, J. N. 1989 Simulation numérique de l'écoulement périodique axisymmétrique dans une cavité cylindrique. *C. R. Acad. Sci. Paris* **308**, 463–469.

Escudier, M. P. 1984 Observations of the flow produced in a cylindrical container by a rotating endwall. *Exps. Fluids* **2**, 189–196.

Gelfgat, A. Yu., Bar-Yoseph, P. Z. & Solan, A. 1996 Stability of confined swirling flow with and without vortex breakdown. *J. Fluid Mech.* **311**, 1–36.

Gelfgat, A. Yu., Bar-Yoseph, P. Z., Solan, A. & Kowalewski, T. A. 1999 An axisymmetry-breaking instability of axially symmetric natural convection. *Intl J. Transport Phenomena* **1**, 173–190.

Gelfgat, A. Yu. & Tanasawa, I. 1993 Systems of basis functions for calculation of three-dimensional fluid flows in cylindrical containers with the Galerkin spectral method. *Proc. Inst. Industrial Science, University of Tokyo, Seisan-Kenkyu* **45**, 60–63.

Goldstein, H. F., Knobloch, E., Mercader, I. & Net, M. 1993 Convection in rotating cylinder. Part 1. Linear theory for moderate Prandtl numbers. *J. Fluid Mech.* **248**, 583–604.

Hardin, G. R., Sani, R. L., Henry, D. & Roux, B. 1990 Buoyancy-driven instability in a vertical cylinder: binary fluids with Soret effect. Part 1. General theory and stationary stability results. *Intl J. Numer. Meth. Fluids* **10**, 79–117.

Jones, C. A. & Moore, D. R. 1979 The stability of axisymmetric convection. *Geophys. Astrophys. Fluid Dyn.* **11**, 245–270.

Lopez, J. M. 1990 Axisymmetric vortex breakdown. Part 1. Confined swirling flow. *J. Fluid Mech.* **221**, 533–552.

Lopez, J. M. & Perry A. D. 1992 Axisymmetric vortex breakdown. Part 3. Onset of periodic flow and chaotic advection. *J. Fluid Mech.* **234**, 449–471.

Neumann, G. 1990 Three-dimensional numerical simulation of buoyancy-driven convection in vertical cylinders heated from below. *J. Fluid Mech.* **214**, 559–578.

Roesner, K. G. 1990 Recirculation zones in a cylinder with rotating lid. In *Topological Fluid Mechanics* (ed. H. K. Moffat & A. Tsinober), pp. 699–708. Cambridge University Press.

Spohn, A., Mory, M. & Hopfinger E. J. 1998 Experiments on vortex breakdown in a confined flow generated by a rotating disc. *J. Fluid Mech.* **370**, 73–99.

Stevens, J. L., Lopez, J. M. & Cantwell, B. J. 1999 Oscillatory flow states in an enclosed cylinder with a rotating endwall. *J. Fluid Mech.* **389**, 101–118.

Tsitverblit, N. & Kit, E. 1998 On the onset of nonsteadiness in confined vortex flows. *Fluid Dyn. Res.* **23**, 125–152.

Wanschura, M., Kuhlmann, H. C., & Rath, H. J. 1996 Three-dimensional instability of axisymmetric buoyant convection in cylinders heated from below. *J. Fluid Mech.* **326**, 399–415.